ARMY RESEARCH LABORATORY

Real-time Intelligent Chemical and Biological Nanosensors on Flexible Platform - II

by Govind Mallick and Shashi P. Karna

ARL-TR-4769 **March 2009**

NOTICES

Disclaimers

The findings in this report are not to be construed as an official Department of the Army position unless so designated by other authorized documents.

Citation of manufacturer's or trade names does not constitute an official endorsement or approval of the use thereof.

Destroy this report when it is no longer needed. Do not return it to the originator.

Army Research Laboratory
Aberdeen Proving Ground, MD 21005-5069

ARL-TR-4769 **March 2009**

Real-time Intelligent Chemical and Biological Nanosensors on Flexible Platform - II

Govind Mallick and Shashi P. Karna
Weapons and Materials Research Directorate, ARL

REPORT DOCUMENTATION PAGE

Form Approved
OMB No. 0704-0188

1. REPORT DATE *(DD-MM-YYYY)*	2. REPORT TYPE	3. DATES COVERED (From - To)
March 2009	Final	10/1/07 to 09/30/08

4. TITLE AND SUBTITLE
Real-time Intelligent Chemical and Biological Nanosensors on Flexible Platform - II

5a. CONTRACT NUMBER

5b. GRANT NUMBER

5c. PROGRAM ELEMENT NUMBER

6. AUTHOR(S)
Govind Mallick and Shashi P. Karna

5d. PROJECT NUMBER

5e. TASK NUMBER

5f. WORK UNIT NUMBER

7. PERFORMING ORGANIZATION NAME(S) AND ADDRESS(ES)
U.S. Army Research Laboratory
ATTN: AMSRD-ARL-WM
Aberdeen Proving Ground, MD 21005-5069

8. PERFORMING ORGANIZATION REPORT NUMBER
ARL-TR-4769

9. SPONSORING/MONITORING AGENCY NAME(S) AND ADDRESS(ES)

10. SPONSOR/MONITOR'S ACRONYM(S)

11. SPONSOR/MONITOR'S REPORT NUMBER(S)

12. DISTRIBUTION/AVAILABILITY STATEMENT
Approved for public release; distribution unlimited.

13. SUPPLEMENTARY NOTES

14. ABSTRACT
In this report, we investigate the current rectification property of chemical vapor deposited (CVD), as-grown single-walled carbon nanotubes (SWNTs). We use the long strands of SWNT bundles to fabricate multiple arrays of switching devices with channel lengths of 3, 5, 7, and 10 μm on a 15 x 15 mm^2 silicon dioxide (SiO_2) on silicon (Si) substrate. A majority of the fabricated devices, regardless of channel length, showed current rectification characteristics with high throughput of current (*I*) in the forward bias (*V*). Atomic force microscopic (AFM) analysis of the device structure and surface topology of SWNTs suggests the observed rectification of current results from surface irregularities and is possibly due to change in the chirality of a single tube. Using fabricated SWNT field-effect transistors (FETs), we have demonstrated the effects of gases, particularly O_2 and N_2, on the fabricated devices.

15. SUBJECT TERMS
Rectification, chemical vapor deposition, single-wall CNT

16. SECURITY CLASSIFICATION OF:			17. LIMITATION OF ABSTRACT	18. NUMBER OF PAGES	19a. NAME OF RESPONSIBLE PERSON
a. REPORT	b. ABSTRACT	c. THIS PAGE			Govind Mallick
Unclassified	Unclassified	Unclassified	UU	22	19b. TELEPHONE NUMBER (*Include area code*) 410-306-1901

Standard Form 298 (Rev. 8/98)
Prescribed by ANSI Std. Z39.18

Contents

List of Figures

Acknowledgments

We gratefully acknowledge the contributions of Dr. Mark Griep (Michigan Technical University), Dr. Sangeeta Sahoo (Rensselaer Polytechnic Institute), Dr. Sarah Lastella (Vishay Technology), and Professor Pulickel Ajayan (Rice University) for their significant contributions in this project. We also wish to thank Mr. Samuel Hirsch of the U.S. Army Research Laboratory (ARL), Weapons and Materials Research Directorate (WMRD) for help with the scanning electron microscope (SEM) characterizations. This research was made possible by the Director's Research Initiatives, ARL-DRI-07-WMR-10 and ARL-DRI-08-WMR-10.

INTENTIONALLY LEFT BLANK.

1. Objectives

The objectives of this research are to examine the feasibility of real-time sensing of chemical and biological species by using the unique materials and electronic properties of carbon nanotubes, and to demonstrate, when possible, the multi-agent sensing and information processing capabilities of such devices. The specific goals of the present research are as follows:

1. To understand and develop process flow for single-walled carbon nanotube (SWNT) growth with desired electronic properties.
2. To fabricate electronic devices using the SWNTs and characterize their electrical properties.
3. To demonstrate single and possibly multiple chemical agent sensing and detection properties of SWNT nanoelectronic devices.

2. Background

Current rectification by SWNT has been predicted from theoretical calculations (*1*, *2*) and has also been observed in a number of previous experiments (*3*–*6*). Theoretical predictions suggest the cross or Y-type junctions, atomic defect, and/or changes in chirality along the tube axis can lead to current rectification due to Schottky-type junctions. Experimental observations have been made on Y-type junctions (*4*) with tubes having different diameters forming the junction, chemical doping of the tubes (*5*), as well as double-gate electrostatic doping of tubes (*6*), effectively creating a p-n junction along a single tube.

Rectifiers have important applications in military as well as commercial electronics as radio signal detectors and AC-to-DC power converters. In order to realize nanoscale electronics and microsystems, it is critically important to develop materials and establish mechanisms for nanoscale current rectification. As a first step toward realizing nanoscale rectifiers, we have investigated the current (*I*)–voltage (*V*) characteristics of chemical vapor deposited (CVD)-grown, SWNT field-effect transistors (FETs). Here we present the results of our study showing current rectification by "as-grown" SWNT devices without external doping. We propose the diode-like property due to the hybrid chirality of single tubes.

The electronic structure of nanotubes depends on their diameter and helicity (*7*, *8*). They can be either metallic or semiconducting, depending on the arrangements of the phenyl rings. The armchair carbon nanotubes (CNTs) are metallic, whereas the zigzag can be either metallic (1/3) or semiconducting (2/3) (*9*, *10*). Theoretically, these different helices can be joined together in a

single-wall nanotube through a linear junction, hence creating a diode-like property (*1, 11*). In general, diode-like behavior in nanotubes is caused by creating an energy barrier at the junction by changing the internal structure of the tube. However, this type of behavior is seldom seen in CVD-processed CNTs. Typically, they show either a metallic or semi-conductive behavior (*12, 13*). Here, we report asymmetric/diode behavior in the *I–V* characteristics of CVD-grown SWNTs, possibly due to the internal defects.

The main objective of this project was to explore and demonstrate the feasibility of SWNT-based, real-time, multi-agent chemical and biological sensors on a flexible platform. Here, we also report a successful demonstration of single chemical agent (N_2 and O_2) sensing and detection properties of SWNT nanoelectronic devices.

3. Approach

Our approach consisted of three distinct parts:

1. Process optimization for the growth of switchable SWNT on technologically compatible substrates
2. Fabrication and electrical characterization of SWNT switching devices
3. Chemical agent sensing and detection with the use of fabricated SWNT electronic devices

In the first year of the proposed research, we accomplished the fabrication of functional switching devices, thus completing the first two parts. The third part, the sensing and detection of chemical species, particularly the sensitivity of gases (O_2 and N_2) was performed during the second year.

4. Experiments

SWNTs are grown using a metal nanoparticle catalyzed CVD process (*13*). The CNT-CVD synthesis procedure uses methane (CH_4) gas as the feedstock carbon source. We used iron (Fe)-nanoparticles as the catalyst for CNT growth and a Fe-nanoparticle-coated, 100-nm-thick silicon oxide (SiO_2) layer on heavily doped silicon (Si) as the substrate. We placed the catalyst nanoparticle-coated substrate inside the tube oven and heated to 920 °C under a constant argon flow (~50 sccm) and pressure of 500 Torr. Upon reaching the set-point temperature, we maintained the system at these conditions for 10 min to ensure that the environment inside the tube furnace was stable. Finally, the argon flow was turned off and the methane flow was simultaneously initiated at a rate of ~100 sccm. After 5 min, we stopped the growth by turning off the methane flow, evacuating the system to 200 mTorr, and allowing the system to cool to

room temperature over a period of 2.5 h. This CVD technique coupled with a novel catalyst system allows relative control of the nanotube properties and alignment such that the final product could be easily converted into a working device. We performed surface characterizations of the as-grown SWNT samples using an atomic force microscope (AFM) (CP-II, Veeco).

We fabricated the devices by photolithographically depositing a 100-nm layer of gold (Au) on top of 10-nm-thick titanium (Ti) to serve as electrodes with varying source (S) and drain (D) separation. The dimension of each electrode pad was 250 x 250 μm. Each device was uniquely labeled, distinguishing its channel length and its respective row and column. The samples were then annealed at 200 °C for 30 min in constant flow of nitrogen to eliminate possible oxide defects. We then analyzed the post-fabricated devices using a scanning electron microscope (SEM) (Hitachi S-4700) to investigate the structure of the devices and the gaps between the electrodes, and we used the AFM to locate the bridging carbon nanotubes between the electrodes under ambient conditions. We were able to locate bundles of SWNTs connecting the pads with all four gap devices. A single substrate with an approximate size of 15 x 15 mm^2 comfortably housed 135 devices. These substrates included four different types with a channel length (gap) between the electrodes of 3, 5, 7, and 10 μm, respectively. We probed the electrical properties of the assembled devices by using *I–V* measurements with a semiconductor (SC) analyzer (Janis/Keithley-4200) attached to a four-probe micro-manipulated cryogenic system.

We tested the electrical sensitivity of gases on the fabricated devices using the high vacuum chamber of the SC analyzer. Current with respect to voltage were measured using the two probe system in vacuum and concurrently in pure O_2 and N_2 (100%) gases, respectively.

5. Results and Discussions

Figure 1 presents the AFM image and height profile of as-grown SWNTs on a 10 x 10 μm^2 Si/SiO_2 substrate. As indicated by the height profile, the SWNTs are 2 to 3 nm in height, which corresponds to the approximate known diameter of SWNTs. Interestingly, we found the width of the imaged SWNTs to be ~100 nm, indicating aligned bundles of SWNTs. Atomic resolution images of part of the nanotube, shown in figure 2, reveal that each CNT strand shown in figure 1 is, in fact, a bundle of several single nanotubes aligned parallel to each other. For one segment (figure 2a) of a nanotube bundle, the AFM scan shown in figure 2 (b, c, and d) exhibits four individual nanotubes aligned parallel to each other, with an individual diameter of ~2 nm each in a scan area of 20 x 20 nm^2. In figure 2b, the first tube displays smooth and cylindrical walls, while the three remaining tubes are distorted and exhibit discontinuity on the tube wall. This is made clear in figure 2d, which is the height image of figure 2b in terms of two color regimes. A closer examination of the two central tubes in figure 2b further reveals that the tubes are twisted on their respective axis. As described by Dumitrica et al. (*14*), the bonds of nanotubes can either

snap in a brittle fashion or they may stretch and deform. However, the intrinsic properties of the tubes play a major role in the breakage. For example, the intrinsic twist or chirality of the tube can create strain and stress to the neighboring bonds, resulting in bond cleavage.

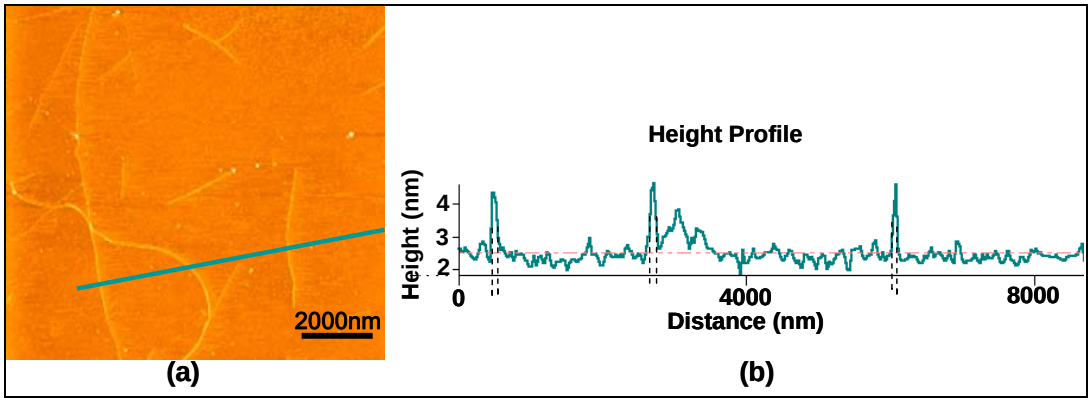

Figure 1. (a) AFM topographical image (10 x 10 μm^2) of as-grown CVD SWNTs and (b) the related height profile.

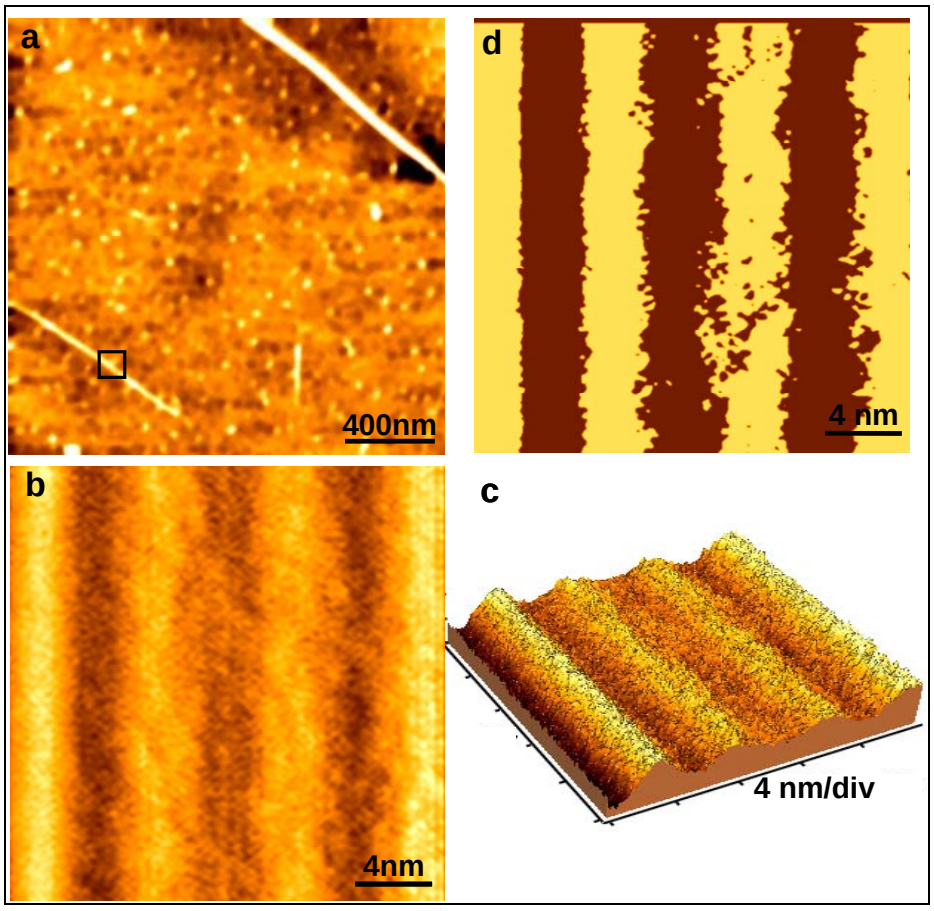

Figure 2. (a) AFM topographical image of 2 x 2 μm^2 scan area, (b) partial atomic resolution AFM topographical image of the area indicated in (a), (c) 3-D image of (b), and (d) filtered image of (b) differentiating the topography in two color regime showing the defects in SWNTs.

Some of the devices, specifically those near the edges of the substrate, were damaged and could not be probed. Of the 135 fabricated devices, 103 were probed, of which 35% were found to be active in this particular sample. Out of these active devices 61% of 3 μm-gap, 28% of 5 μm-gap, 22% of 7 μm-gap, and 26% of 10 μm-gap devices were found active, i.e., they showed measurable electrical characteristics. A majority of the active devices (72%) showed asymmetric *I–V* curves and the rest were either metallic or had no observable electrical activity due to lack of connecting tubes.

Figure 3 shows a typical *I–V* curve of a fabricated SWNT device obtained from a two-probe measurement. The *I–V* curve shown is for a 7-μm channel length device (lower inset). The upper inset is the *I–V* curve on a 7-μm length control device with no SWNT in the channel. The left lower inset shows the scanning electron micrograph of the device layout.

Furthermore, the SWNT diodes gave high throughput of current in the forward bias (figure 3). The forward/reverse current ratio (I_{for}/I_{rev}) was in the order of 10^6. The asymmetric behavior is possibly due to the internal defect, as shown in figure 4, which is the exposed atomic resolution image of second strand of SWNT bundle in figure 2. The analysis reveals that the tube is twisted significantly. Here a part of the graphene sheet as a layer of nanotube wall is super imposed on the AFM atomic resolution image. This shows the distinction where one part of the sheet has armchair (n,n) chirality and the other part is zigzag (n,0). This chirality alteration is most likely due to the twisting of the nanotube. It is a well-documented fact that the armchair tubes have a virtually negligible energy gap compared to the zigzag (*15*). Thus, a tube with mixed chirality gives rise to a potential barrier at the junction of the dissimilar chiral structures, resulting in asymmetric current under biased condition.

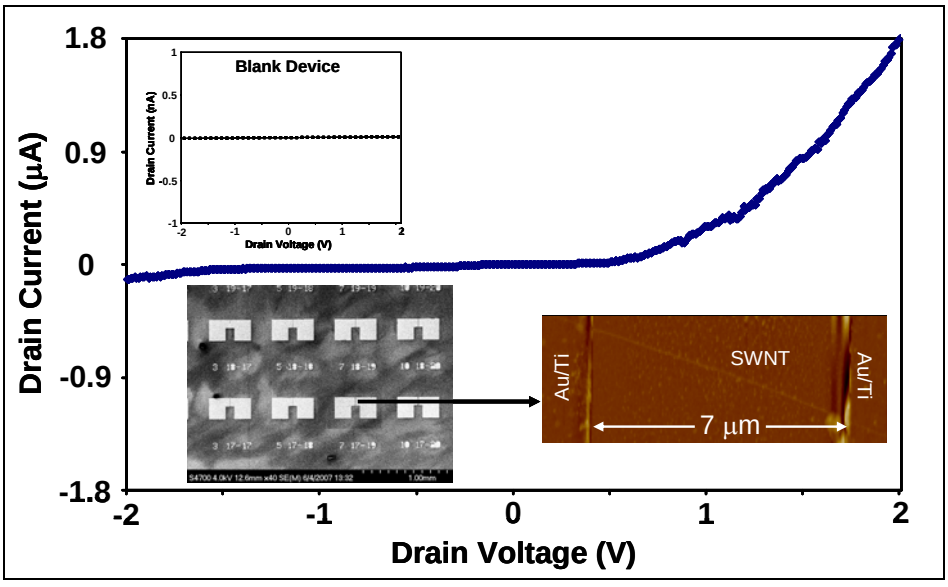

Figure 3. Two-terminal *I–V* measurement of 7 μm-gap device: the lower insets show the SEM image of different device patterns and an AFM image of 2.5 x 10 μm^2 scan area showing SWNTs connecting the two electrode pads and the upper left inset shows the *I–V* measurement of a blank 7 μm-gap device.

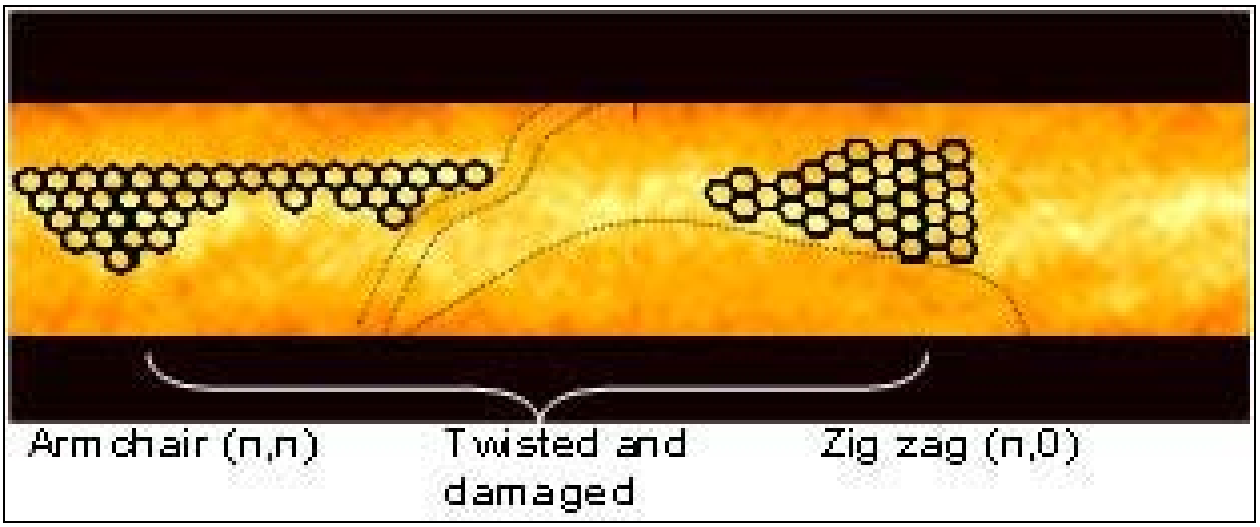

Figure 4. Atomically resolved AFM image (10 x 2 nm^2) of a single strand of SWNT; the dotted lines show the twisting and possible fragments of bonds.

The possibility of a unimolecular SWNT diode has been discussed in previous studies (*2–5*). Since our devices also consisted of cross junctions with varying tube diameters (AFM image, not shown here) along different arms as well as bundles with mixed metallic-semiconducting tubes, it is important to consider the possible mechanism of the observed rectification. The notable possibilities are the cross junctions of tubes with metallic and semi-conducting properties, contributions due to tube electrode junctions, and single tubes with morphological non-uniformity including atomic level defects, tube wall deformation, and mixed chirality along the tube length. We cannot conclusively exclude the contributions from cross-junction tubes due to the observed presence of such junctions in some of our devices. However, since our device use symmetric electrodes (Au on both sides), we may exclude the effect of dissimilar electrodes. For the same reason (symmetric electrodes), we believe that the difference in tube electrode contact resistance at the two junctions has little or no contribution to the observed rectification. This leaves us with the possibility of a Schottky diode with channels consisting of SWNTs with different work functions, and possibly, a different electronic structure.

Figure 5 summarizes the current and its voltage derivative (conductance) as a function of applied voltage dominant diode type SWNT devices fabricated in this study. Clearly, the magnitude of the drain current is significantly higher at the positive bias compared to the negative bias indicating pure diode properties of the devices. The open device architecture used in the present work led us to explore the chemical agent sensing properties of SWNT devices, as described in the next section.

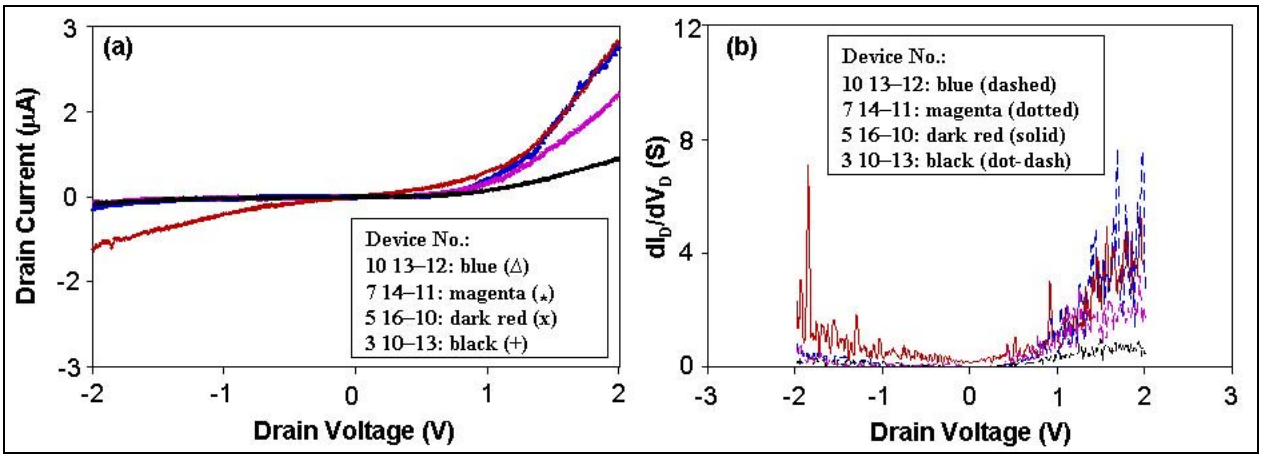

Figure 5. (a) Two-terminal *I–V* measurements of four different gap devices and (b) their respective conductance plot.

Figure 6 (a–d) show the *I–V* characteristics of the fabricated device in the presence of N_2 and O_2 gases. Also included in the figure are the *I–V* measurements in ambient (labeled air) and in vacuum. Figure 6 (a–d) corresponds to devices with (a) dominantly metallic channel, (b) semiconducting SWNT, (c) Schottky-type diode with low current, and (d) high-current output Schottky diode. The *I–V* characteristics of the devices exhibit the expected response due to the material properties of SWNTs. For example, the *I–V* characteristics of the metallic channel (figure 6a) exhibit very little change in presence/absence of gases. This is expected, since the adsorption of gases on the SWNT surface hardly change the already high conductivity of metallic tubes. On the other hand, the *I–V* characteristics of a semiconducting device (figure 6b), which experiences substantial modification in the carrier concentration due to the adsorption of N_2 and O_2 gases, exhibit maximum changes. The SWNT channels with diode type characteristics (figures 6c and 6d) exhibit changes in their *I–V* characteristics intermediate between those of the metallic (figure 6a) and semiconducting (figure 6b) devices. In each case however, the magnitude of current increases in the presence of both gases. This is clear in all types of SWNTs, i.e., metallic, semi-conducting, and rectifying. However, the SWNTs show no or minimal effect in air as compared to vacuum.

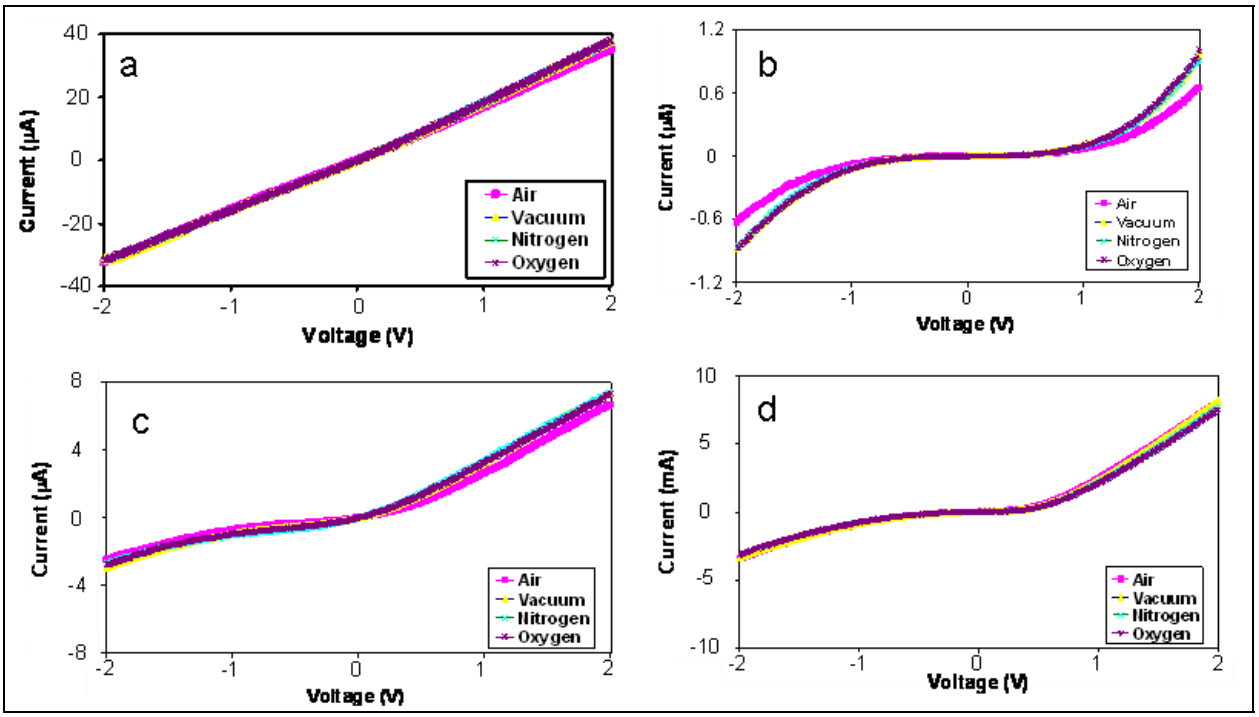

Figure 6. The gas effect on SWNTs (a) metallic, (b) semiconductor, (c) rectifier, and (d) high current (mA) rectifier.

6. Summary and Conclusion

In summary, we have grown SWNTs by CVD process and fabricated arrays of SWNT electronic switches in open channel configurations. A majority of the devices fabricated with the "as-grown" SWNT exhibited prominent rectification characteristics (I_{for}/I_{rev} ~10^6). We also demonstrated the sensitivity of SWNTs in the presence of different gases, as well as demonstrated the fabrication of arrayed patterns of SWNT switching devices on a single chip. The present process is compatible with the current industry-standard Si-electronics and could be easily transitioned for mass fabrication of the SWNT switching devices. The increase in current magnitude in presence of oxygen and nitrogen shows that the devices composed of SWNTs can be used in sensor applications.

7. References

1. Treboux, G.; Lapstun, P.; Silverbrook, K. An Intrinsic Carbon Nanotube Heterojunction Diodes. *J. Phys. Chem. B* **1999**, *103*, 1871–1875.
2. Srivastava, D.; Menon, M.; Ajayan, P. M. Branched Carbon Nanotube Junctions Predicted by Computational Nanotechnology and Fabricated through Nanowelding. *J. Nanoparticle Res.* **2003**, *5*, 395–400.
3. Collins, P. G.; Zettl, A.; Bando, H.; Thess, A.; Smalley, R. E. Nanotube Nanodevice. *Science* **1997**, *278*, 100–103.
4. Satishkumar, B. C.; Thomas, P. J.; Govindraj, A.; Rao, C.N.R. Y-Junction Carbon Nanotubes. *Appl. Phys. Lett.* **2000**, *77*, 2530–2532.
5. Zhou, C.; Kong, J.; Yenilmez, E.; Dai, H. Modulated Chemical Doping of Individual Carbon Nanotubes. *Science* **2000**, *290*, 1552–1555.
6. Lee, J. U.; Gipp, P. P.; Heller, C. M. Carbon Nanotube p-n Junction Diodes. *Appl. Phys. Lett.* **2004**, *85*, 145–147.
7. Saito, R.; Fujita, M.; Dresselhaus, G.; Dresselhaus, M. S. Electronic Structure of Chiral Graphene Tubules. *Appl. Phys. Lett*. **1992**, *60*, 2204–2206.
8. Hamada, N.; Sawada, S.; Oshiyama, A. New One-Dimensional Conductors: Graphitic Microtubules. *Phys. Rev. Lett*. **1992**, *68*, 1579–1581.
9. Wildöer, J.W.G.; Venema, L. C.; Rinzler, A. R.; Smalley, R. E.; Dekker, C. Electronic Structure of Atomically Resolved Nanotubes. *Nature* **1998**, *391*, 59–62.
10. Odom, T. W.; Huang, J.; Kim, P.; Lieber, C. M. Atomic Structure and Electronic Properties of Single-Walled Carbon Nanotubes. *Nature* **1998**, *391*, 62–64.
11. Chico, L.; Crespi, V. H.; Benedict, L. X.; Louie, S. G.; Cohen, M. L. Pure Carbon Nanoscale Devices: Nanotube Heterojunctions. *Phys. Rev. Lett*. **1996**, *76*, 971–974.
12. Lastella, S.; Mallick, G.; Woo, R.; Rider, D. A.; Manners, I.; Jung, Y. J.; Ryu, C. Y.; Ajayan, P. M.; Karna, S. P. Parallel Arrays of Individually Addressable Single-walled Carbon Nanotube Field-effect Transistor. *J. Appl. Phys*. **2006**, *99*, 024302 (1)–024302 (4).
13. Lastella, S.; Joon Jung, Y.; Yang, H.; Vajtai, R.; Ajayan, P. M.; Ryu, C. Y.; Rider, D. A.; Manners, I. Density Control of Single-walled Carbon Nanotubes Using Patterned Iron Nanoparticle Catalysts Derived from Phase Separated Thin Films of a Polyferrocene Block Copolymer. *J. Mat. Chem.* **2004**, *14*, 1791–1794.

14. Dumitrica, P.; Hua, M.; Yakobson, B. I. Symmetry-, Time-, and Temperature-Dependent Strength of Carbon Nanotube. *Proceedings of National Academy of Sciences (PNAS)* **2006**, *103* (16), 6105–6109.

15. Ouyang, M.; Huang, J.; Cheung, C. L.; Lieber, C. M. Atomically Resolved Single-Walled Carbon Nanotube Intramolecular Junction. *Science* **2001**, *292*, 97–100.

List of Symbols, Abbreviations, and Acronyms

ARL	U.S. Army Research Laboratory
AFM	atomic force microscope
Au	gold
CH_4	methane
CNTs	carbon nanotubes
CVD	chemical vapor deposition
D	drain
Fe	iron
FETs	field-effect transistors
I	current
MTU	Michigan Technical University
RPI	Rensselaer Polytechnic Institute
S	source
SC	semiconductor
SEM	scanning electron microscope
Si	silicon
SiO_2	silicon dioxide
SWNT	single-walled carbon nanotube
Ti	titanium
V	voltage
WMRD	Weapons and Materials Research Directorate

No. of Copies	Organization
1 (PDF only)	DEFENSE TECHNICAL INFORMATION CTR DTIC OCA 8725 JOHN J KINGMAN RD STE 0944 FORT BELVOIR VA 22060-6218
1 CD	DIRECTOR US ARMY RESEARCH LAB IMNE ALC HRR 2800 POWDER MILL RD ADELPHI MD 20783-1197
1 CD	DIRECTOR US ARMY RESEARCH LAB AMSRD ARL CI OK TL 2800 POWDER MILL RD ADELPHI MD 20783-1197
1 CD	DIRECTOR US ARMY RESEARCH LAB AMSRD ARL CI OK PE 2800 POWDER MILL RD ADELPHI MD 20783-1197
6 HCs	US ARMY RESEARCH LAB ATTN AMSRD ARL SE EI DR K K CHOI ATTN AMSRD ARL SE EM DR PAUL SHEN DR JOSEPH MAIT ATTN AMSRD ARL SE RL DR PAUL AMIRTHARAJ DR MADAN DUBEY DR STEVEN KILPATRICK 2800 POWDER MILL ROAD ADELPHI MD 20783
1 HC	DIRECTOR NIGHT VISION & ELECTRONIC SENSORS DIRECTORATE ATTN AMSRD CER NV 10221 BURBECK ROAD FORT BELVOIR VA 22060-5806
1 HC	NIGHT VISION & ELECTRONIC SENSORS DIRECTORATE ATTN AMSRD CER NV DR JAMES RATCHES 10221 BURBECK ROAD FORT BELVOIR VA 22060-5806
1 HC	NIGHT VISION & ELECTRONIC SENSORS DIRECTORATE ATTN AMSRD CER NV OPS TPP MS JUANIE M URIBE INTL PROG SPECIALIST 10221 BURBECK ROAD FORT BELVOIR VA 22060-5806
1 HC	US ARMY RESEARCH LAB SPECTRUM ANALYSIS & FREQUENCY MANAGEMENT AMSRD CER ST AS FM DR JEFFREY BOKSINER FORT MONMOUTH NJ 07703-5201
1 HC	US ARMY RDECOM AMSRD CER CS DR ARTHUR BALLATO COMM ELECTRONICS RDEC FORT MONMOUTH NJ 07703-5201
1 HC	CERDEC STCD DR DEREK S MORRIS FORT MONMOUTH NJ 07703-5201
1 HC	DIRECTOR US ARMY RDECOM / AMRDEC AMSRD AMR SG NC REDSTONE ARSENAL AL 35898-5254
2 HCs	US ARMY RDECOM / AMRDEC AMSRD AMR SG NC DR PAUL RUFFIN DR JAMES C HOLT REDSTONE ARSENAL AL 35898-5254
1 HC	DIRECTOR CHEMICAL BIOLOGICAL DETECTION US ARMY ECBC RDECOM ATTN AMSRD ECB RT 5183 BLACKHAWK ROAD APG MD 21010-5424
1 HC	CHEMICAL BIOLOGICAL DETECTION ATTN AMSRD ECB RT D DR AUGUSTUS W FOUNTAIN III CHIEF SCIENTIST 5183 BLACKHAWK ROAD APG MD 21010-5424

No. of Copies | Organization

1 HC | US ARMY ECBC RDECOM
ATTN AMSRD ECB RT
DR JAMES J VALDES
SCIENTIFIC ADVISOR FOR
BIOTECHNOLOGY (ST)
5183 BLACKHAWK ROAD
APG MD 21010-5424

1 HC | DIRECTOR
US ARMY NATICK SOLDIER CENTER
ATTN AMSRD NSC
NATICK MA 01760-502

5 HCs | US ARMY NATICK SOLDIER CENTER
ATTN AMSRD NSC SS
DR LYNNE SAMUELSON
ATTN AMSRD NSC SS MS
MR BARRY DECRISTOFANO
DR STEPHEN A FOSSEY
DR BRIAN KIMBALL
DR MARGARET E ROYLANCE
NATICK MA 01760-502

2 HCs | DEFENSE THREAT REDUCTION
AGENCY
STOP 6201
DR SALVATORE R BOSCO
DR CHARLES A BASS
8725 JOHN J KINGMAN ROAD
FORT BELVOIR VA 22060-6201

1 HC | US ARMY MEDICAL RESEARCH
INSTITUTE OF INFECTIOUS DISEASE
DR FRANK J LEBEDA
1425 PORTER AVE
FT DETRICK MD 21702-5011

1 HC | US MILITARY ACADEMY
DEPARTMENT OF CHEMISTRY AND
LIFE SCIENCES
PHOTONIC RESEARCH CENTER
LTC JOHN M INGRAM
BUILDING 753 OFFICE 24B
WEST POINT NY 10996

No. of Copies | Organization

ABERDEEN PROVING GROUND

40 HCs | DIR USARL
1 CD | AMSRD ARL CI OK TP (BLDG 4600
AMSRD ARL WM
DR SHASHI P KARNA (20 copies)
AMSRD ARL WM BD
DR GOVIND MALLICK (20 copies)
APG MD 21005-5069

1 HC | R PAUL H DEITZ
HUMAN RESEARCH AND
ENGINEERING DIRECTORATE
ATTN AMSRD ARL HR
APG MD 21005-5425

TOTAL: 74 (1 PDF, 4 CDs, 69 HCs)

INTENTIONALLY LEFT BLANK.